

ACCEPTED MANUSCRIPT

Glitch subtraction from gravitational wave data using adaptive spline fitting

To cite this article before publication: Soumya D Mohanty *et al* 2023 *Class. Quantum Grav.* in press <https://doi.org/10.1088/1361-6382/acd0fe>

Manuscript version: Accepted Manuscript

Accepted Manuscript is “the version of the article accepted for publication including all changes made as a result of the peer review process, and which may also include the addition to the article by IOP Publishing of a header, an article ID, a cover sheet and/or an ‘Accepted Manuscript’ watermark, but excluding any other editing, typesetting or other changes made by IOP Publishing and/or its licensors”

This Accepted Manuscript is © 2023 IOP Publishing Ltd.



During the embargo period (the 12 month period from the publication of the Version of Record of this article), the Accepted Manuscript is fully protected by copyright and cannot be reused or reposted elsewhere.

As the Version of Record of this article is going to be / has been published on a subscription basis, this Accepted Manuscript will be available for reuse under a CC BY-NC-ND 3.0 licence after the 12 month embargo period.

After the embargo period, everyone is permitted to use copy and redistribute this article for non-commercial purposes only, provided that they adhere to all the terms of the licence <https://creativecommons.org/licenses/by-nc-nd/3.0>

Although reasonable endeavours have been taken to obtain all necessary permissions from third parties to include their copyrighted content within this article, their full citation and copyright line may not be present in this Accepted Manuscript version. Before using any content from this article, please refer to the Version of Record on IOPscience once published for full citation and copyright details, as permissions may be required. All third party content is fully copyright protected, unless specifically stated otherwise in the figure caption in the Version of Record.

View the [article online](#) for updates and enhancements.

Glitch subtraction from gravitational wave data using adaptive spline fitting

Soumya D. Mohanty, Mohammad A. T. Chowdhury

Department of Physics and Astronomy, University of Texas Rio Grande Valley, One West University Blvd., Brownsville, Texas 78520, USA

E-mail: soumya.mohanty@utrgv.edu

E-mail: mohammadabuthaher.chowdhury01@utrgv.edu

Abstract. Transient signals of instrumental and environmental origins (“glitches”) in gravitational wave data elevate the false alarm rate of searches for astrophysical signals and reduce their sensitivity. Glitches that directly overlap astrophysical signals hinder their detection and worsen parameter estimation errors. As the fraction of data occupied by detectable astrophysical signals will be higher in next generation detectors, such problematic overlaps could become more frequent. These adverse effects of glitches can be mitigated by estimating and subtracting them out from the data, but their unpredictable waveforms and large morphological diversity pose a challenge. Subtraction of glitches using data from auxiliary sensors as predictors works but not for the majority of cases. Thus, there is a need for nonparametric glitch mitigation methods that do not require auxiliary data, work for a large variety of glitches, and have minimal effect on astrophysical signals in the case of overlaps. In order to cope with the high rate of glitches, it is also desirable that such methods be computationally fast. We show that adaptive spline fitting, in which the placement of free knots is optimized to estimate both smooth and non-smooth curves in noisy data, offers a promising approach to satisfying these requirements for broadband short-duration glitches, the type that appear quite frequently. The method is demonstrated on glitches drawn from three distinct classes in the Gravity Spy database as well as on the glitch that overlapped the binary neutron star signal GW170817. The impact of glitch subtraction on the GW170817 signal, or those like it injected into the data, is seen to be negligible.

1. Introduction

In a fairly short time since the first direct detection of a gravitational wave (GW) signal (GW150914) in 2015 [1] by the twin LIGO [2] detectors, GW astronomy has emerged as an information-rich field that will revolutionize our understanding of compact objects such as black holes and neutron stars. By now, the network of LIGO and Virgo [3] detectors has reported 90 confirmed detections of GW signals from compact binary coalescences (CBCs) across the first observing run (O1) [4] to the third (O3) [5]. The majority of these are binary black hole (BBH) mergers but the haul also includes a binary neutron star (BNS) system (GW170817) [6].

1 2 *Adaptive spline glitch removal* 2 3

4
5 The rate of detectable GW signals will grow as more detectors, namely KAGRA [7]
6 and LIGO-India [8], join the network and increase its distance reach for GW sources.
7 Design studies are already underway for the successors to the current generation of GW
8 detectors [9, 10, 11] with the goal of achieving an order of magnitude improvement in
9 sensitivity across the current operational frequency band. In addition, next-generation
10 detectors will seek to expand the operational range to lower frequencies (≈ 1 Hz),
11 thereby increasing the duration of in-band GW signals across the board: for example, a
12 BNS signal starting at ≈ 10 Hz will last for days compared to the ≈ 1 min for GW170817.
13 Thus, future detectors will not only see a higher rate but also longer signals, raising the
14 prospect [12] that there will be no data segment free of detectable GW signals.
15

16 The false alarm rate of searches for CBCs as well as generic short duration GW
17 signals, or *bursts*, is dominated [13] by transient non-GW signals of instrumental or
18 environmental origins, commonly called *glitches*. This is because glitches that populate
19 the same frequency band as CBC or burst signals and happen to be transient in duration
20 can falsely trigger the respective search pipelines. A glitch has a particularly adverse
21 effect if it overlaps with a GW signal, as happened in the case of GW170817 [6], and
22 triggers the search pipeline to reject the glitch and possibly discard the signal. Even a
23 non-overlapping glitch can severely degrade parameter estimation if it is close enough to
24 a GW signal [14]. In the third observing run of the LIGO and Virgo detectors, $\approx 20\%$ of
25 detected GW signals overlapped with glitches [15] due to the high glitch rate in Virgo.
26 For future detectors, the frequency of accidental overlaps will be enhanced by the higher
27 rate of detectable GW signals as well as, for CBC signals, their longer durations.
28

29 Glitches have dissimilar and unpredictable waveforms but many of the observed ones
30 tend to fall into distinct morphological classes. This has motivated the investigation of
31 automated glitch classification using machine learning where a range of different methods
32 have been proposed, such as Support Vector Machine [16], t-Sne [17], random forests [16],
33 S-means [18], and Deep Convolutional Neural Networks [19]. The Gravity Spy [20]
34 project uses a citizen science approach to engage the lay public in labeling glitches by
35 visual inspection of their constant Q-transform (CQT) [21, 22] time-frequency images.
36 This has created a high quality training dataset for machine learning methods. By now,
37 more than 20 named glitch classes are available in the Gravity Spy database, collected
38 over multiple observing runs of the LIGO detectors [17].
39

40 Several different approaches have been developed to mitigate the adverse effects
41 of glitches on GW searches. GW search pipelines typically compute secondary
42 functionals, called *veto*es, of the data besides the primary detection statistic that help
43 in distinguishing genuine GW signals from glitches. A well-known example is the Chi-
44 square veto [23] used in CBC search pipelines. For LIGO-Virgo data, a set of Data
45 Quality flags have been developed that use information from a large number of auxiliary
46 sensors to quantify the safety of analyzing a given segment of GW strain data [24]. For
47 glitches that overlap a GW signal, the gating [25] method removes the rectangular time-
48 frequency block, or just the time interval, containing an identified glitch from the data.
49 Cross-channel regression using data from auxiliary sensors [26, 27, 28, 29] has been
50

1
2 *Adaptive spline glitch removal* 3
34 used to reduce excess broadband noise and a few types of glitches [30].
56 A relatively recent approach is that of estimating the waveform of a glitch
7 from the data time series itself and subtracting it out. Glitch subtraction was of
8 critical importance in the case of GW170817 and has been shown to be an important
9 requirement in reducing bias in the estimation of GW signal parameters [31]. The
10 GW170817 glitch subtraction was carried out using the multi-detector BayesWave
11 pipeline [32, 33], which has also been used for other types of glitches [15]. Another
12 method, Glitschen [34], follows the approach of constructing parametrized waveform
13 models for identified glitch classes using principal component analysis of training sets.
14 A strong motivation for developing glitch estimation and subtraction methods is that
15 one could, in principle, preprocess the data to clean out every sufficiently loud glitch of
16 a known type. As exemplified by GW170817, where prior subtraction of the loud glitch
17 would have kept the search pipeline from discarding the signal, this would make glitch
18 rejection in all downstream GW searches safer.
1920 In this paper, we present a method for the estimation and subtraction of broadband,
21 short-duration glitches that have appeared frequently in the observation runs of the
22 LIGO detectors. The method is computationally cheap, works with single-detector
23 data, does not require a training set of pre-identified glitches, and is not predicated on
24 auxiliary sensor data. The core component of the method is SHAPES (Swarm Heuristics
25 based Adaptive and Penalized Estimation of Splines), an adaptive spline curve fitting
26 algorithm introduced in [35]‡. SHAPES uses splines with free placement of knots to fit
27 both smooth and non-smooth curves in noisy data. In particular, point discontinuities
28 in the curve or its derivatives (up to some order) can be accommodated in the fit by
29 allowing knots to merge. The ability to handle both sharp and slow changes in a curve
30 is a built-in form of multiresolution analysis in SHAPES and a critical requirement for
31 effective estimation of broadband glitches. We examine the performance of our glitch
32 subtraction method on the GW170817 glitch in LIGO-Livingston data and instances of
33 glitches from three morphologically distinct classes, namely, *Blip*, *Koi Fish*, and *Tomte*,
34 in the Gravity Spy database. In each of the latter three cases, we inject a BNS signal
35 overlapping with the glitch to mimic the case of GW170817. We find that the impact
36 of glitch subtraction on the signals, real or injected, is negligible.
3738 The rest of the paper is organized as follows. Sec. 2 reviews SHAPES with the
39 goal of providing a self-contained description of the algorithm that is pertinent to this
40 paper. Further details, such as the motivation and justification for certain features of
41 the algorithm, can be found in [35]. Sec. 3 describes the dataset used in this paper and
42 the details of how SHAPES is used for glitch subtraction. Sec. 4 presents the results.
43 Our conclusions and discussion of future work are presented in Sec. 5.
4445

‡ The SHAPES code is available from the Github repository [mohanty-sd/SHAPES.git](https://github.com/mohanty-sd/SHAPES.git).

1
2 *Adaptive spline glitch removal*
3
4
5
6

7 **2. Adaptive spline fitting: the SHAPES algorithm**
8
9

10 SHAPES is derived under the following models for the noisy data, \bar{y} , and the signal
11 $\bar{s}(\theta)$.
12
13

$$\bar{y} = \bar{s}(\theta) + \bar{\epsilon}, \quad (1)$$

14 where \bar{y} , \bar{s} , and $\bar{\epsilon}$ are row vectors with N elements, $y_i = y(t_i)$ and $s_i(\theta) = s(t_i; \theta)$,
15 $i = 0, 1, \dots, N - 1$, are samples taken at $t_i = i/f_s$ with f_s being the sampling frequency,
16 and θ denotes the set of signal parameters that need to be estimated from the data. The
17 noise samples, ϵ_i , are drawn independently from the zero mean and unit variance normal
18 (Gaussian) probability density function $N(0, 1)$. The white Gaussian noise assumption
19 does not entail a loss of generalization since GW data can always be whitened using the
20 estimated noise power spectral density (PSD).
21

22 The signal $s(t; \theta)$ is assumed in SHAPES to be a cubic spline, which is a polynomial
23 of order 4. The choice of a spline model as well as its order is an ad hoc one, with only
24 an empirical justification, since a rigorous approach requires restricting the class of
25 functions being estimated but this may be difficult for glitches. A cubic spline can be
26 represented by a linear combination of B-spline functions [36],
27

$$s(t; \theta = \{\bar{\alpha}, \bar{\tau}\}) = \sum_{j=0}^{P-5} \alpha_j B_{j,4}(t; \bar{\tau}), \quad (2)$$

32 where $\bar{\alpha} = (\alpha_0, \alpha_1, \dots, \alpha_{P-5})$, and $\bar{\tau} = (\tau_0, \tau_1, \dots, \tau_{P-1})$, $\tau_{i+1} \geq \tau_i$, is a sequence
33 of P *knots* that marks the end points of the contiguous intervals containing the
34 polynomial pieces of the spline. Note that knots are allowed to be equal, leading to
35 knots with multiplicity higher than one. (The knots τ_0 and τ_{P-1} are repeated 3 times
36 each.) The number of B-splines in Eq. 2 corresponds to the number of independent
37 parameters describing the spline after the continuity and differentiability constraints on
38 the polynomial pieces at the interior knots are taken into account. Repeating knots
39 create discontinuity in either the value of a B-spline function or its derivatives (up to
40 order 2). This allows the $s(t; \theta)$ in Eq. 2 to model signals with point discontinuities
41 in value or derivatives. Fig. 1 illustrates cubic B-spline functions for an ad hoc knot
42 sequence.
43
44

45 The best fit spline parameters, $\hat{\alpha}$ and $\hat{\tau}$, are those that minimize a penalized least-
46 squares function,
47

$$L_\lambda(\bar{\alpha}, \bar{\tau}) = L(\bar{\alpha}, \bar{\tau}) + \lambda R(\bar{\alpha}), \quad (3)$$

$$L(\bar{\alpha}, \bar{\tau}) = \sum_{i=0}^{N-1} (y_i - s_i(\bar{\alpha}, \bar{\tau}))^2, \quad (4)$$

54 where the penalty term,
55

$$R(\bar{\alpha}) = \sum_{j=0}^{P-5} \alpha_j^2, \quad (5)$$

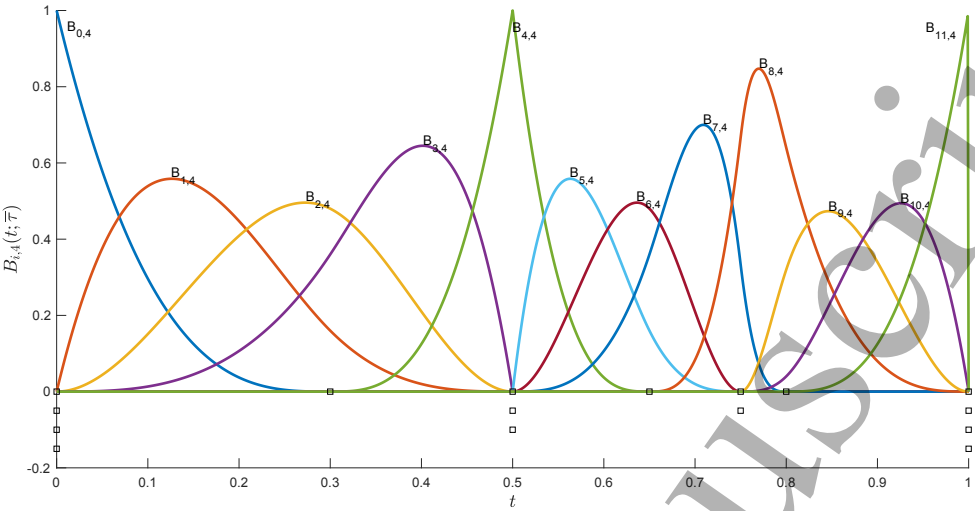
1
2 *Adaptive spline glitch removal*
3
4
5
6
7
8
9
10
11
12
13
14
15
16
17
18
19
20
21
22
23
24
25
26
27
28
29
30
31
32
33
34
35
36
37
38
39
40
41
42
43
44
45
46
47
48
49
50
51
52
53
54
55
56
57
58
59
60

Figure 1. Cubic B-spline functions $B_{j,4}(t; \bar{\tau})$, $j = 0, 1, \dots, 11$, for an arbitrary choice of 16 knots $(\bar{\tau})$ marked by squares. Knots with multiplicity > 1 result in B-splines that are discontinuous in value or derivatives.

is found to be useful in the suppression of spurious clustering of the knots. These clusters are observed when the method tries to minimize $L_\lambda(\bar{\alpha}, \bar{\tau})$ by fitting out outlier data points arising from the noise alone. The strength of the penalty is controlled by the gain factor λ , with higher values of λ leading to smoother estimates.

The optimization of $L_\lambda(\bar{\alpha}, \bar{\tau})$ over the non-linear parameters $\bar{\tau}$ has been a long-standing computational barrier [37, 38, 39, 40] for adaptive spline fitting. At the same time, the benefits of optimizing the placement of knots have also been demonstrated extensively [38, 41]. It was shown in [42], and independently in [43], that Particle Swarm Optimization (PSO) [44, 45], a widely used nature-inspired metaheuristic for global optimization, has good performance on the free knot placement problem. Moreover, being a continuous optimization method, PSO can explore all arrangements of knots, including the ones where knots are sufficiently close to be merged into a single knot of higher multiplicity. This allows the fitting of functions that have a mix of smooth and non-smooth parts.

There are many variations [46] among the algorithms that fall under the umbrella of the PSO metaheuristic but they all share the following common features. (i) They are continuous optimization methods that seek the global optimum of a function $f(\bar{x})$, $\bar{x} \in \mathbb{D} \subset \mathbb{R}^K$, called the *fitness function*, on an open subset \mathbb{D} , called the *search space*, of the space \mathbb{R}^K of real K -tuples. (In the case of SHAPES, the search space coordinates \bar{x} are the knots $\bar{\tau}$.) The function is sampled at multiple locations, called *particles*, that move iteratively to explore the search space for the global optimum. The set of particles is called a *swarm*. (ii) The location of each particle is updated following a dynamical rule that typically uses the best location found by a particle in its history, called its *personal best*, and the best location found by the particles in its *neighborhood*, called its *local best*. Here, the fitness value at a location defines how good it is: for a minimization problem,

1
2 *Adaptive spline glitch removal* 6
34
5 the lower the fitness, the better the location. A common form of the dynamical rule
6 computes the displacement of a particle by linearly combining three vectors: its previous
7 displacement and the two vectors pointing from its current position to the personal and
8 local best locations. However, the linear combination is performed with an independent
9 random weight for each component of the latter two vectors. (iii) Each particle explores
10 the search space independently but is constantly attracted towards the personal and
11 local bests. This leads to a form of communication between the particles that speeds
12 up convergence to a promising region, followed by refinement of the solution until the
13 iterations are terminated. The PSO algorithm can avoid trapping by local minima due
14 to both the randomness in the dynamical rule and the parallel exploration of the search
15 space by the swarm.
1617
18 The best location among all the particles at termination is the final solution found
19 by the swarm for the global optimum. While there is no guarantee that the final solution
20 is the true global optimum, the probability of successful convergence can be boosted
21 exponentially by running multiple independent runs of PSO and picking the one with
22 the best final solution. Most of the parameters involved in the PSO algorithm, such
23 as the number of particles or the weights attached to the attractive forces, have very
24 robust values across a wide variety of benchmark optimization problems [47] and rarely
25 need to be changed. In our experience, there are typically only two quantities that
26 need tuning: the number of iterations, N_{iter} , to termination and the hyper-parameter
27 N_{runs} , the number of independent PSO runs. In this paper, we fix $N_{\text{iter}} = 2000$ and
28 $N_{\text{runs}} = 8$ throughout. The number of particles is always set to 40 and the settings for
29 the remaining parameters, as well as the definition of the neighborhood used for the
30 local best, are described in [35].
3132
33 The description above was for the case where the number of knots, P , is fixed. The
34 complete SHAPES algorithm incorporates model selection using the Akaike Information
35 Criterion (AIC) [48], where the optimum number of knots minimizes,
36

37
$$\text{AIC} = 4P + L_{\lambda}(\hat{\alpha}, \hat{\tau}) . \quad (6)$$

38

39
40 While, given sufficient computing resources, model selection could be performed over all
41 values of P until the minimum value of AIC is found, practical considerations dictate
42 that the set of knot numbers used be a finite and small one. In this paper, for example,
43 we use knot numbers in the set starting at 5 and ending at 60 in increments of 5. It is
44 important to note that this restriction of knot numbers is not a fundamental limitation
45 but a technical one meant to manage the computational burden of model selection.
46 Thus, the only significant free parameter that needs to be set by the user in the current
47 version of SHAPES is λ .
4849
50 Since SHAPES assumes that the noise in the data is white, GW strain data must
51 be whitened prior to glitch estimation and subtraction. The data conditioning steps
52 involved are as follows (in sequential order). (a) Suppression of the seismic noise
53 below 10 Hz, (b) robust estimation of the power spectral density (PSD) noise floor,
54 (c) whitening of the noise floor using the estimated PSD [49], and (d) automated
5556
57
58
59
60

1
2 *Adaptive spline glitch removal*
3
4
5
6
7
8
9

identification of high-power narrowband noise features (“lines”) and their suppression using notch filters. These steps are common to all GW search pipelines, so they do not need to be elaborated further here.

10 **3. Demonstration data**
11
12

The glitches considered in this paper for demonstrating the performance of SHAPES are listed in Table 1. The corresponding GW strain data files can be located and downloaded from the Gravitational Wave Open Science Center (GWOSC) [50] using the information provided in this table. We have used the standard 4096 sec long GWOSC data files sampled at 4 kHz.

The GW170817 glitch presents a particularly interesting example of the deleterious effect of glitches on GW searches. The GW signal appeared in both LIGO-Hanford (H1) and LIGO-Livingston (L1) with a combined network signal to noise ratio (SNR) of 32.4. Such a strong signal would have been detected easily in coincidence across L1 and H1 by the GW search pipelines in operation at the time. However, a coincident detection was prevented by a large overlapping glitch in L1 causing the release of only an unusual single-detector GW detection alert to the astronomical community. About 4.5 hours elapsed between the initial alert and the release of the first skymap localizing GW170817 obtained by gating the glitch.

In addition to the GW170817 glitch, we have taken three representative glitches from the Blip, Koi Fish, and Tomte, classes in the Gravity Spy database [51]. These glitches were selected by taking the loudest 5 events, in terms of their signal-to-noise ratio (SNR) as given in the Gravity Spy database, for each class and then picking the first one in this list for which the corresponding GWOSC file had 100% science data that was also reasonably stationary. As can be seen from Table 1, this results in the selected glitches spanning a wide range in SNR.

Glitch Name	GPS start (sec)	SNR	Detector	run
GW170817 glitch	1187008880	–	L1	O2
Blip	1182397347	109.1	H1	O2
Koi Fish	1169847108	608.1	H1	O2
Tomte	1173086299	19.6	H1	O2

41
42 **Table 1.** Glitches considered in this paper along with their GPS start times, SNRs,
43 the detectors in which they appeared, and the observation runs. For the Blip, Koi Fish,
44 and Tomte glitches, the start times are taken from the Gravity Spy database. To the
45 best of our knowledge, there is no SNR available in the literature for the GW170817
46 glitch.
47
48
49
50
51
52
53
54

55 After conditioning the data, we use the start time of a glitch, recorded in Table 1,
56 to locate the glitch. Starting from the peak of the glitch, the data time series is scanned
57 visually in both directions to identify a segment, containing the glitch, that tapers off
58 at both its boundaries to the general noise level of the conditioned data.
59
60

1
2 *Adaptive spline glitch removal* 8
3
4
5
6
7
8
9
10
11
12
13
14
15
16
17

To mimic the case of GW170817 and to study the effect of glitch subtraction on an overlapping GW signal, we injected a whitened restricted-2PN circularized binary inspiral signal with equal $1.4 M_{\odot}$ components in the conditioned data. The SNR (in white noise with unit variance) of the injected signal is set at 37.3, which is an ad hoc factor of $\sqrt{2}$ higher than the observed SNR of 26.4 of GW170817 in L1 [6]. The enhancement in SNR allows clearer visibility of the signal in time-frequency images while also posing a stronger challenge to SHAPES in terms how well it ignores the GW signal when estimating a glitch. The segment containing the glitch, taken from the conditioned data with the injected signal, is passed to SHAPES for estimation of the glitch waveform followed by its subtraction.

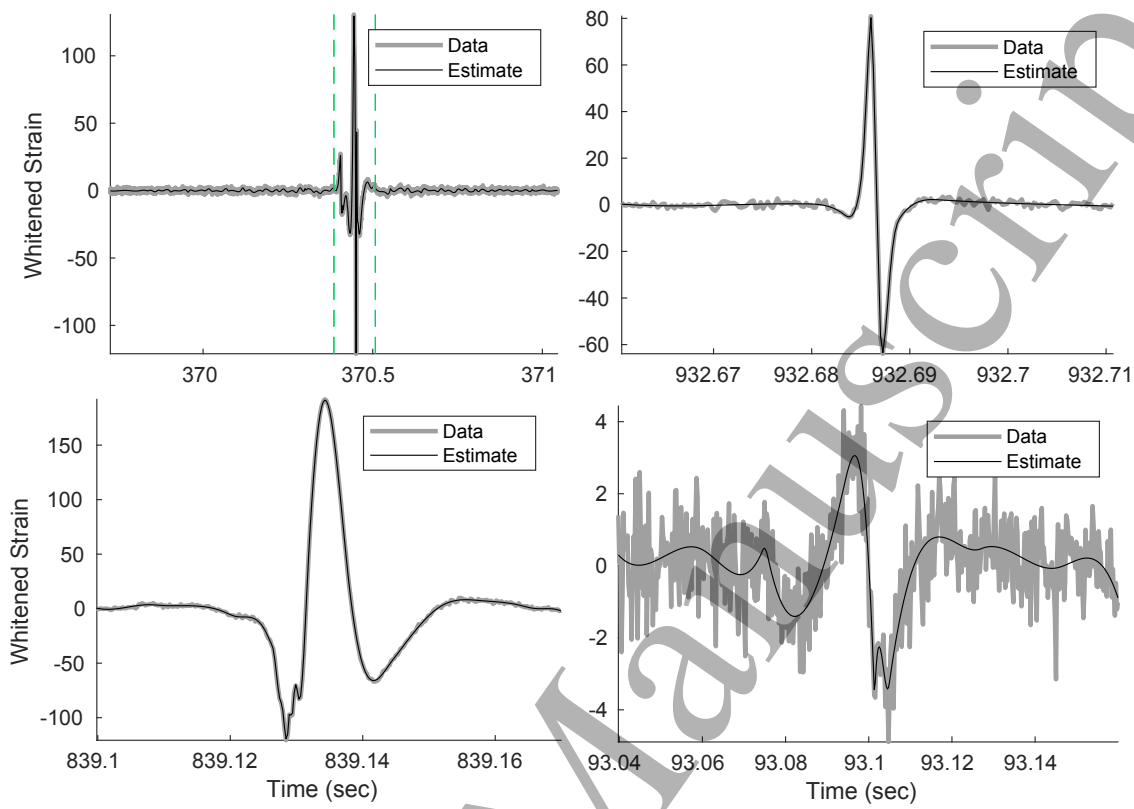
18
19 **4. Results**
20
21

In common with other papers on glitch estimation and subtraction, we present our results in the form of CQT time-frequency images and time series plots. These are obtained by taking projections of the data on a set of windowed sinusoids. The width of the window decreases with an increase in the carrier frequency, f_c , such that $Q = f_c/\Delta f$, where Δf is the -3 dB bandwidth of the Fourier transform of the window, remains constant. We use the CQT code provided in the `librosa` [52] Python package for audio processing. For each glitch, we show CQTs of the conditioned data with injected signal and the residual after subtraction of the glitch estimate.

Fig. 2 shows the data segments that were processed using SHAPES and the corresponding estimated glitch waveforms. Except for GW170817, each segment was processed as a whole to obtain the glitch estimate. In the case of GW170817, SHAPES was applied independently to three separate but contiguous time intervals to estimate the complete glitch. This was necessitated by the presence of extended wings, preceding and trailing the core broadband (and rapidly varying) part in the middle, that dominate the conditioned data for ≈ 0.5 sec on each side. Applying SHAPES to the complete segment would have required using a very large number of knots (> 60), making it unnecessarily expensive computationally given that splitting the segment achieves a good solution.

As mentioned in Sec. 2, the penalty gain λ controls the smoothness of the estimate and is a user-specified parameter of the SHAPES algorithm. Typically, when a glitch is loud and has a complex shape, $\lambda = 0.01$ allows SHAPES to provide a better fit. For low SNR and simple glitch waveforms, or if the data is just plain white noise, $\lambda = 0.1$ does an adequate job. In general, estimates from SHAPES are not sensitive to small variations of λ around these values because the model selection is able to compensate for a lower value of λ by selecting a higher knot number and vice versa. Without much fine tuning, we found that the values of λ listed in Table 2 work well for the glitches studied in this paper. We have also listed in this table the number of knots for the best fit models selected by the AIC.

Fig. 3 to Fig. 6 show the CQTs of the conditioned data and residuals after glitch

1
2 *Adaptive spline glitch removal*
3
4

32 **Figure 2.** The conditioned strain data and the glitch waveform estimated by SHAPES
33 for each of the glitches considered in this paper. Top row: GW170817 (left) and Blip
34 (right). Bottom row: Koi Fish (left) and Tomte (right). The X-axis in each plot shows
35 the time (sec) since the start of the open data file containing the glitch as provided
36 by GWOSC. For GW170817, the dashed vertical lines demarcate the three adjacent
37 segments that were analyzed separately.

Glitch Name	Penalty gain (λ)	Number of knots
GW170817 glitch	0.1, 0.01, 0.1	60,40,50
Blip	0.01	15
Koi Fish	0.01	30
Tomte	0.1	15

55 **Table 2.** The penalty gain λ used for the glitches and the number of knots in the best
56 fit model. For the GW170817 glitch, there are three segments with the middle one
57 containing the principal glitch and adjacent ones containing the wings. The penalty
58 gains and best fit model are listed for all three segments in sequential order from left
59 to right.

1
2 *Adaptive spline glitch removal* 10
3
4
5
6
7
8
9
10
11
12
13
14
15
16
17
18
19
20

subtraction for the glitches in the sequence GW170817, Blip, Koi Fish, and Tomte, respectively. In all cases, we see that the subtraction of the glitch does not affect the overlapping GW signal (real or injected) in any significant way. Some overfitting to the data, seen as very small CQT values, is visible in the residual for the GW170817 glitch at frequencies below ≈ 32 Hz but this band has no overlap with the signal. The overfitted parts are the two wings of the GW170817 glitch mentioned earlier. The CQTs of the residuals for the Blip and Tomte glitches show near perfect removal of the glitch. (For Tomte, the coalescence time of the GW signal was kept further away from the glitch in order to create an overlap between the signal track and the glitch.) The residual for Koi Fish shows effective removal of the glitch with the exception of a transient and low frequency narrowband component. This leftover component does not overlap with the signal.

For the GW170817 glitch, it is possible to compare the performance of SHAPES with BayesWave directly since the residual from the latter has been provided at GWOSC. (This is the version 2 data for this event from the L1 detector.) Fig. 7 shows the outputs of passing the two residuals through matched filters corresponding to the same BNS parameters. For this experiment, the matched filter templates are from the same family that we have used for injections but the parameters are tuned to be close to the ones estimated for GW170817, namely, the two masses are set at $1.46 M_{\odot}$ and $1.3 M_{\odot}$. (Since our conditioning pipeline is not identical to that used in LIGO, some tuning of the template parameter values is required to get a reasonable output SNR.) As can be seen, the peak values and their arrival times agree well with each other, demonstrating that SHAPES has essentially the same effect on the signal as BayesWave.

The principal computational cost in SHAPES is the global optimization of the fitness function in Eq. 3. The time taken by the current MATLAB [53] code for a single PSO run on a segment with ≈ 300 samples and knot numbers $P \in [10, 60]$ (in steps of 5) is $\lesssim 10$ min on an Intel Xeon E5 processor (clock rate 3 GHz). The runtime increases with the number of knots used, mainly due to an increase in the number of B-spline functions that need to be computed. With a code currently under construction in the C language, and implementation of further hardware acceleration (e.g., using Graphics Processing Units), the runtime is expected to decrease substantially. We also note that the segments containing glitches can be processed in parallel since SHAPES is a purely time-domain method. Hence, the computational cost will scale slower than linearly with the number of glitches when analyzing data containing multiple glitches.

51 **5. Discussion and Conclusions**
52
53
54
55
56
57
58
59
60

We have presented a new approach to glitch subtraction using an adaptive spline fitting method called SHAPES. The method was demonstrated on the GW170817 glitch as well as other representative short duration and broadband glitches. In a single detector and in the absence of strong prior information about the signal, it is not possible to distinguish a GW signal from a glitch in the part where they overlap. Hence, it is

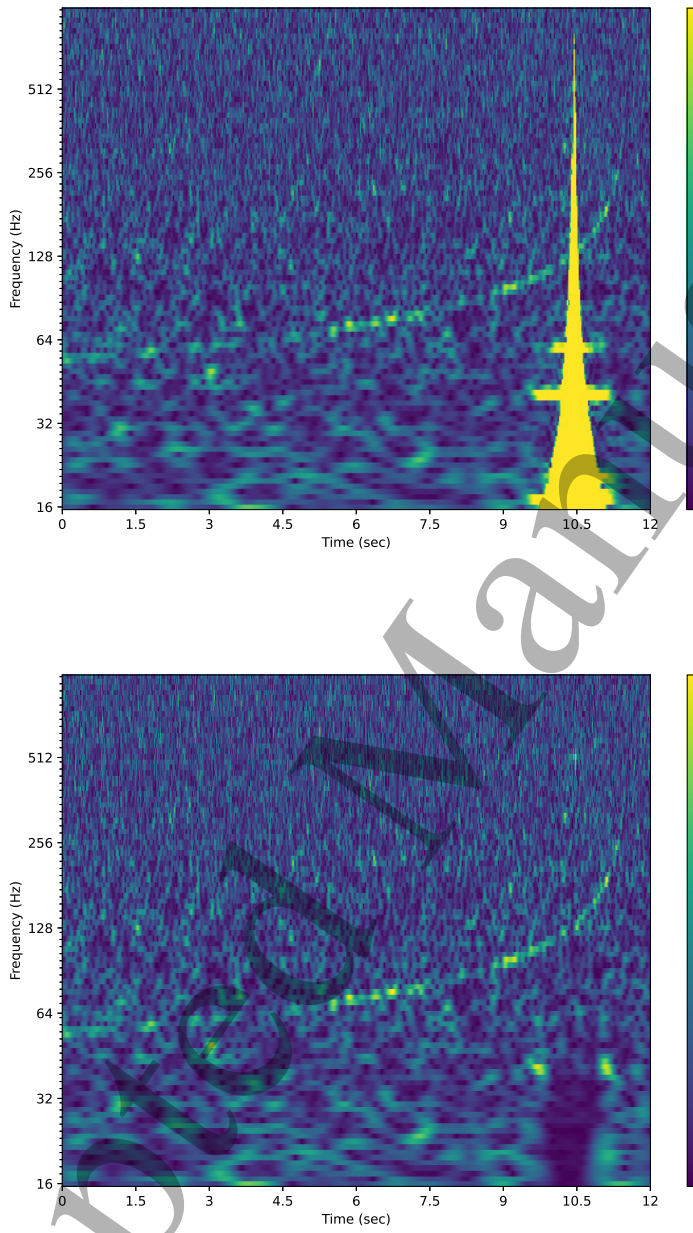
1
2 *Adaptive spline glitch removal*
3
4
5
6
7
8
9
10
11
12
13
14
15
16
17
18
19
20
21
22
23
24
25
26
27
28
29
30
31
32
33
34
35
36
37
38
39
40
41
42
43
44
45
46
47
48
49
50
51
52
53
54
55
56
57
58
59
60

Figure 3. Subtraction of the GW170817 Glitch. The top and bottom panels show the CQT of the data and residual, respectively. The glitch is the vertical feature at ≈ 10.5 sec. In order to show both the glitch and the signal in the same image, a threshold has been applied to the CQT as indicated by the maximum value in the colorbar of the top panel.

expected that the signal power will be removed in that part along with the glitch when the latter is estimated and subtracted out. Nonetheless, as far as the BNS signal used in this paper is concerned, we observe very little impact on the signal across a wide range of glitch SNRs.

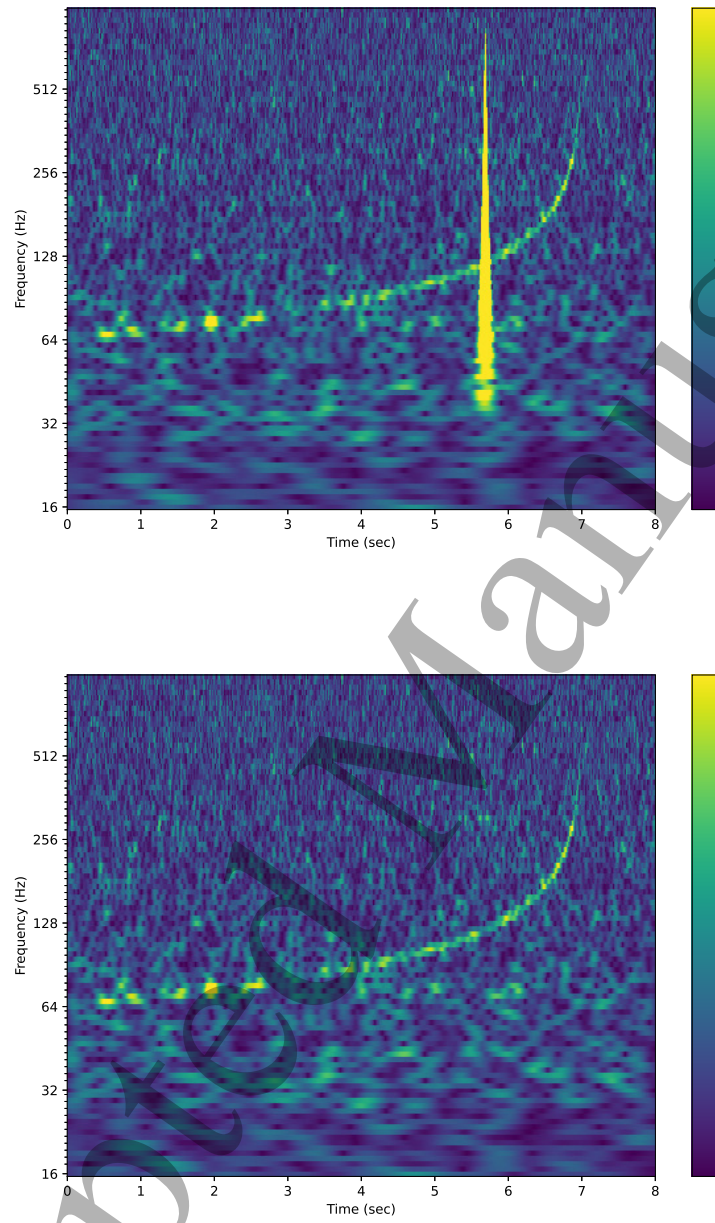
1
2 *Adaptive spline glitch removal*
3
4
5
6
7
8
9
10
11
12
13
14
15
16
17
18
19
20
21
22
23
24
25
26
27
28
29
30
31
32
33
34
35
36
37
38
39
40
41
42
43
44
45
46
47
48
49
50
51
52
53
54
55
56
57
58
59
60

Figure 4. Subtraction of the Blip Glitch. The top and bottom panels show the CQT of the data and residual, respectively. The glitch is the vertical feature at ≈ 6 sec. In order to show both the glitch and the signal in the same image, a threshold has been applied to the CQT as indicated by the maximum value in the colorbar of the top panel.

SHAPES is not well adapted to fitting highly oscillatory waveforms since these are not represented well by splines without using an inordinate number of knots. Therefore, the direct use of SHAPES for glitches in the Gravity Spy database such as whistlers or wandering lines is not viable. However, chirp signals such as these could be

1
2 *Adaptive spline glitch removal*
3
4
5
6
7
8
9
10
11
12
13
14
15
16
17
18
19
20
21
22
23
24
25
26
27
28
29
30
31
32
33
34
35
36
37
38
39
40
41
42
43
44
45
46
47
48
49
50
51
52
53
54
55
56
57
58
59
60

13

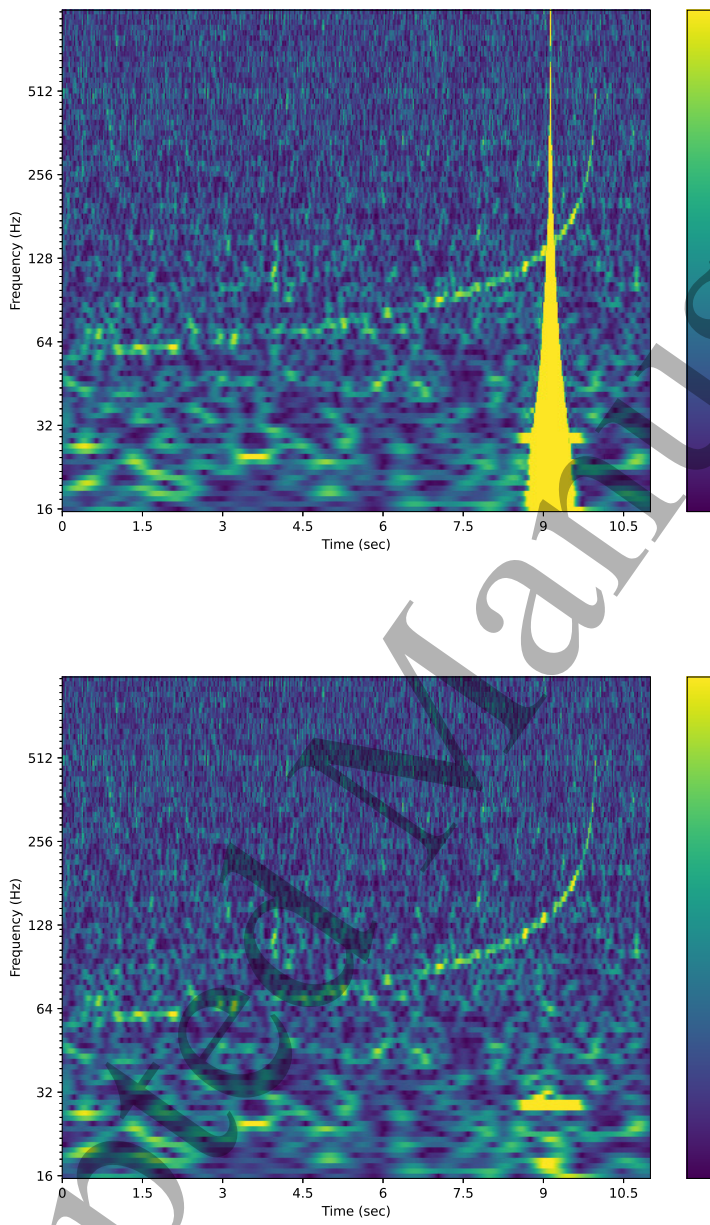


Figure 5. Subtraction of the Koi Fish glitch. The top and bottom panels show the CQT of the data and residual, respectively. The glitch is the vertical feature at ≈ 9.0 sec. In order to show both the glitch and the signal in the same image, a threshold has been applied to the CQT as indicated by the maximum value in the colorbar of the top panel.

estimated using the method proposed in [54, 55], where adaptive splines figure indirectly in a non-linear signal model. This is an interesting direction that will be pursued in future work.

Other current limitations of SHAPES, which are technical in nature, are that the

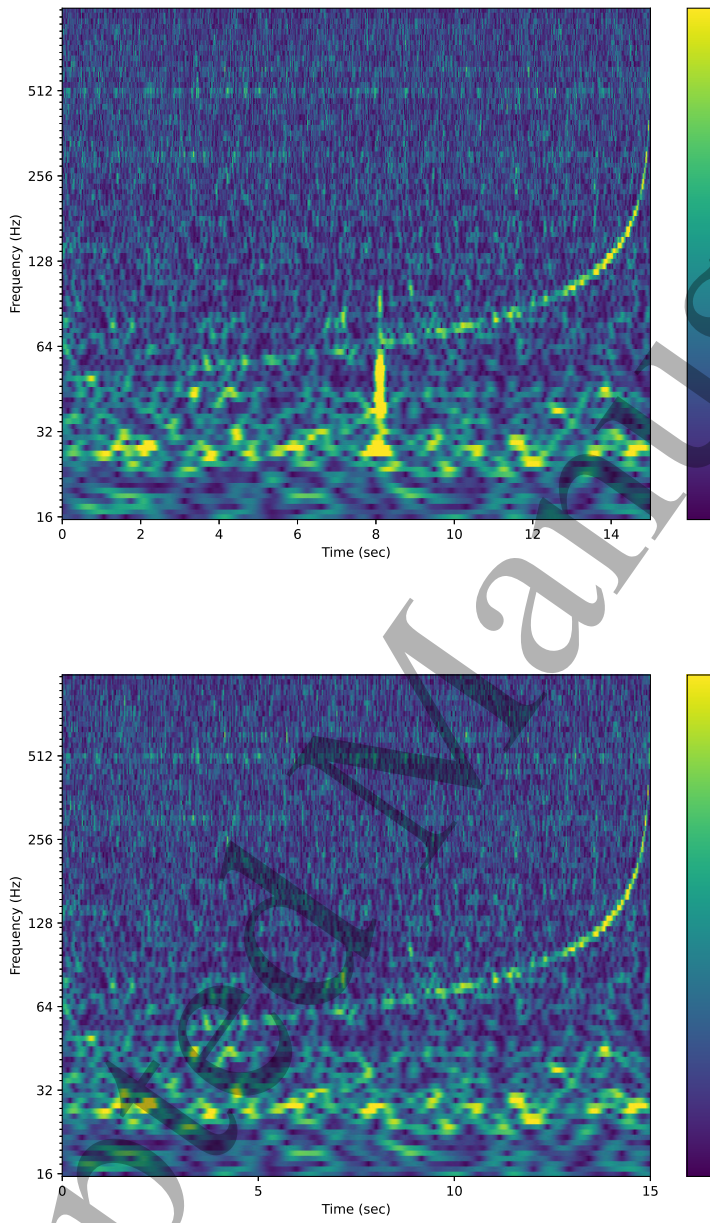
1
2 *Adaptive spline glitch removal*
3
4
5
6
7
8
9
10
11
12
13
14
15
16
17
18
19
20
21
22
23
24
25
26
27
28
29
30
31
32
33
34
35
36
37
38
39
40
41
42
43
44
45
46
47
48
49
50
51
52
53
54
55
56
57
58
59
60

Figure 6. Subtraction of the Tomte Glitch. The top and bottom panels show the CQT of the data and residual, respectively. The glitch is the vertical feature at ≈ 8.0 sec. In order to show both the glitch and the signal in the same image, a threshold has been applied to the CQT as indicated by the maximum value in the colorbar of the top panel.

penalty gain parameter λ as well as the segment length to be processed must be specified by the user. The choice of the latter, along with the nature of the data, influences the number of knots used in the fit and led to the necessity of breaking up the data for the GW170817 glitch into three ad hoc parts. Work is in progress to address both of these

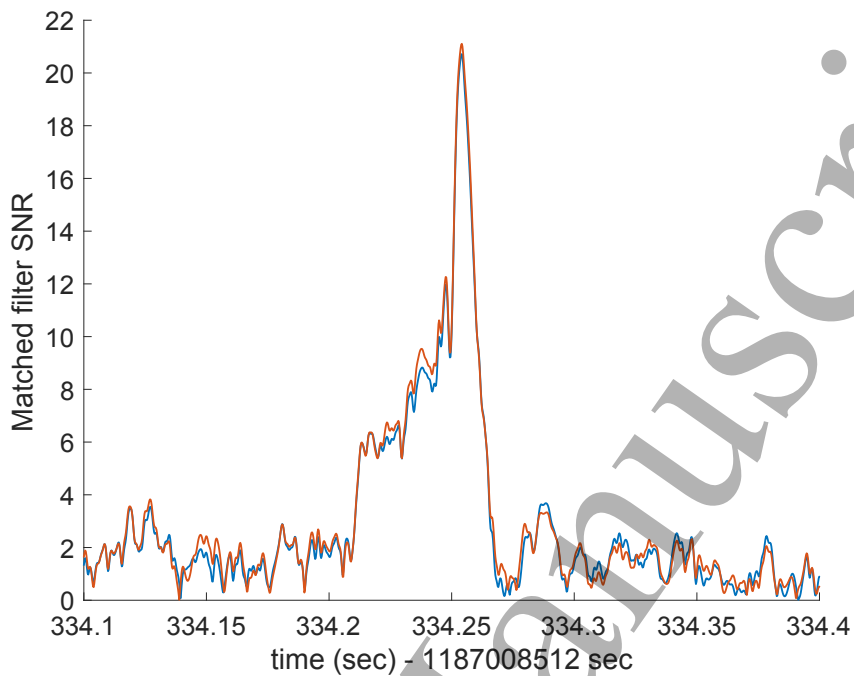
1
2 *Adaptive spline glitch removal*
3
4
5
6
7
8
9
10
11
12
13
14
15
16
17
18
19
20
21
22
23
24
25
26
27
28
29
30
31
32
33
34
35
36
37
38
39
40
41
42
43
44
45
46
47
48
49
50
51
52
53
54
55
56
57
58
59
60

Figure 7. SNR time series outputs of matched filters with identical parameters on the SHAPES (blue) and BayesWave (red) residuals for the GW170817 L1 data. The peak values in both time series occur close to the time at which the instantaneous frequency of the signal crosses 35 Hz.

limitations.

Our results show that SHAPES is a promising addition to the toolbox of glitch subtraction methods that will become increasingly important as GW detectors become more sensitive. SHAPES is computationally inexpensive, taking on the order of a few minutes for each glitch, and will be made much faster by planned code improvements. This could allow, in principle, the subtraction of a large number of broadband glitches of known types as part of data conditioning and provide significantly cleaner data for any type of GW search.

The data set used in this paper and codes for plotting glitch data and SHAPES estimates are provided in a public data release on Zenodo [56].

Acknowledgments

S.D.M is supported by U.S. National Science Foundation (NSF) grant PHY-2207935 and partially supported by the U.S. Department of Defense grant W911NF2110169. MATC acknowledges support from the Presidential Graduate Research Award at the University of Texas Rio Grande Valley. We acknowledge the Texas Advanced Computing Center (TACC) at the University of Texas at Austin (www.tacc.utexas.edu) for providing high performance computing resources.

1
2 *Adaptive spline glitch removal* 16
3
45 **References**
6

- [1] B. P. Abbott et al. (LIGO Scientific Collaboration and Virgo Collaboration). Observation of gravitational waves from a binary black hole merger. *Physical Review Letters*, 116:061102, Feb 2016.
- [2] J. Aasi, et al. (The LIGO Scientific Collaboration). Advanced LIGO. *Classical and Quantum Gravity*, 32:074001, 2015.
- [3] F. Acernese et al. (Virgo Collaboration). Advanced Virgo: a second-generation interferometric gravitational wave detector. *Classical and Quantum Gravity*, 32:024001, 2015.
- [4] B. P. Abbott et al. (LIGO Scientific Collaboration and Virgo Collaboration). GWTC-1: A gravitational-wave transient catalog of compact binary mergers observed by ligo and virgo during the first and second observing runs. *Physical Review X*, 9(3):031040, 2019.
- [5] R. Abbott, et al. (The LIGO Scientific Collaboration, the Virgo Collaboration, the KAGRA Collaboration). GWTC-3: Compact Binary Coalescences Observed by LIGO and Virgo During the Second Part of the Third Observing Run. *arXiv e-prints*, page arXiv:2111.03606, 2021.
- [6] B. P. Abbott et al. (LIGO Scientific Collaboration and Virgo Collaboration) GW170817: Observation of gravitational waves from a binary neutron star inspiral. *Physical Review Letters*, 119:161101, 2017.
- [7] T. Akutsu et al. (KAGRA Collaboration). KAGRA: 2.5 Generation Interferometric Gravitational Wave Detector. *Nature Astron.*, 3:35, 2019.
- [8] C. S. Unnikrishnan. IndIGO and LIGO-India: Scope and plans for gravitational wave research and precision metrology in India. *International Journal of Modern Physics D*, 22(01):1341010, 2013.
- [9] M Punturo et al. The Einstein Telescope: a third-generation gravitational wave observatory. *Classical and Quantum Gravity*, 27(19):194002, 2010.
- [10] Sheila Dwyer, Daniel Sigg, Stefan W. Ballmer, Lisa Barsotti, Nergis Mavalvala, and Matthew Evans. Gravitational wave detector with cosmological reach. *Physical Review D*, 91:082001, Apr 2015.
- [11] Benjamin P Abbott, R Abbott, TD Abbott, MR Abernathy, K Ackley, C Adams, P Addesso, RX Adhikari, VB Adya, C Affeldt, et al. Exploring the sensitivity of next generation gravitational wave detectors. *Classical and Quantum Gravity*, 34(4):044001, 2017.
- [12] Tania Regimbau, Thomas Dent, Walter Del Pozzo, Stefanos Giampanis, Tjonne G. F. Li, Craig Robinson, Chris Van Den Broeck, Duncan Meacher, Carl Rodriguez, B. S. Sathyaprakash, and Katarzyna Wójcik. Mock data challenge for the Einstein gravitational-wave telescope. *Phys. Rev. D*, 86:122001, 2012.
- [13] B P Abbott et al. Effects of data quality vetoes on a search for compact binary coalescences in advanced LIGO's first observing run. *Classical and Quantum Gravity*, 35:065010, 2018.
- [14] Jade Powell. Parameter estimation and model selection of gravitational wave signals contaminated by transient detector noise glitches. *Classical and Quantum Gravity*, 35(15):155017, 2018.
- [15] Derek Davis, TB Littenberg, IM Romero-Shaw, M Millhouse, J McIver, F Di Renzo, and G Ashton. Subtracting glitches from gravitational-wave detector data during the third observing run. *Classical and Quantum Gravity*, 39(24):245013, 2022.
- [16] Rahul Biswas, Lindy Blackburn, Junwei Cao, Reed Essick, Kari Alison Hodge, Erotopoulos Katsavounidis, Kyungmin Kim, Young-Min Kim, Eric-Olivier Le Bigot, Chang-Hwan Lee, John J. Oh, Sang Hoon Oh, Edwin J. Son, Ye Tao, Ruslan Vaulin, and Xiaoge Wang. Application of machine learning algorithms to the study of noise artifacts in gravitational-wave data. *Phys. Rev. D*, 88:062003, Sep 2013.
- [17] S. Bahaadini, V. Noroozi, N. Rohani, S. Coughlin, M. Zevin, J.R. Smith, V. Kalogera, and A. Katsaggelos. Machine learning for Gravity Spy: Glitch classification and dataset. *Information Sciences*, 444:172–186, 2018.
- [18] S Mukherjee, R Obaid, and B Matkarimov. Classification of glitch waveforms in gravitational

1
2 *Adaptive spline glitch removal* 17
3

- 4 wave detector characterization. *Journal of Physics: Conference Series*, 243:012006, aug 2010.
- 5 [19] Daniel George, Hongyu Shen, and E. A. Huerta. Classification and unsupervised clustering of ligo
6 data with deep transfer learning. *Phys. Rev. D*, 97:101501, 2018.
- 7 [20] Michael Zevin, Scott Coughlin, Sara Bahaadini, Emre Besler, Neda Rohani, Sarah Allen, Miriam
8 Cabero, Kevin Crowston, Aggelos K Katsaggelos, Shane L Larson, et al. Gravity spy:
9 integrating advanced ligo detector characterization, machine learning, and citizen science.
10 *Classical and Quantum Gravity*, 34(6):064003, 2017.
- 11 [21] Judith C Brown. Calculation of a constant Q spectral transform. *The Journal of the Acoustical
12 Society of America*, 89(1):425–434, 1991.
- 13 [22] S Chatterji, L Blackburn, G Martin, and E Katsavounidis. Multiresolution techniques for the
14 detection of gravitational-wave bursts. *Classical and Quantum Gravity*, 21(20):S1809, 2004.
- 15 [23] Bruce Allen. χ^2 time-frequency discriminator for gravitational wave detection. *Physical Review
16 D*, 71:062001, Mar 2005.
- 17 [24] BP Abbott et al. Characterization of transient noise in Advanced LIGO relevant to gravitational
18 wave signal GW150914. *Classical and Quantum Gravity*, 33(13):134001, 2016.
- 19 [25] S. A. Usman et al. An improved pipeline to search for gravitational waves from compact binary
20 coalescence. *Classical and quantum gravity*, 33:215004, 2016.
- 21 [26] B. Allen, W. Hua, and A. Ottewill. Automatic cross-talk removal from multi-channel data. *ArXiv
22 General Relativity and Quantum Cosmology e-prints*, September 1999.
- 23 [27] Jennifer C Driggers, Matthew Evans, Keenan Pepper, and Rana Adhikari. Active noise
24 cancellation in a suspended interferometer. *Review of Scientific Instruments*, 83(2):024501,
25 2012.
- 26 [28] V Tiwari, M Drago, V Frolov, S Klimenko, G Mitselmakher, V Necula, G Prodi, V Re, F Salemi,
27 G Vedovato, and I Yakushin. Regression of environmental noise in LIGO data. *Classical and
28 Quantum Gravity*, 32(16):165014, 2015.
- 29 [29] G. Vajente, Y. Huang, M. Isi, J. C. Driggers, J. S. Kissel, M. J. Szczepańczyk, and S. Vitale.
30 Machine-learning nonstationary noise out of gravitational-wave detectors. *Phys. Rev. D*,
31 101:042003, Feb 2020.
- 32 [30] J. C. Driggers et al. Improving astrophysical parameter estimation via offline noise subtraction
33 for Advanced LIGO. *Phys. Rev. D*, 99:042001, Feb 2019.
- 34 [31] Chris Pankow, Katerina Chatzioannou, Eve A. Chase, Tyson B. Littenberg, Matthew Evans,
35 Jessica McIver, Neil J. Cornish, Carl-Johan Haster, Jonah Kanner, Vivien Raymond, Salvatore
36 Vitale, and Aaron Zimmerman. Mitigation of the instrumental noise transient in gravitational-
37 wave data surrounding GW170817. *Phys. Rev. D*, 98:084016, Oct 2018.
- 38 [32] Neil J. Cornish and Tyson B. Littenberg. Bayeswave: Bayesian inference for gravitational wave
39 bursts and instrument glitches. *Classical and Quantum Gravity*, 32(13):135012, 2015.
- 40 [33] Katerina Chatzioannou, Neil Cornish, Marcella Wijngaarden, and Tyson B. Littenberg. Modeling
41 compact binary signals and instrumental glitches in gravitational wave data. *Phys. Rev. D*,
42 103:044013, Feb 2021.
- 43 [34] JD Merritt, Ben Farr, Rachel Hur, Bruce Edelman, and Zoheyr Doctor. Transient glitch mitigation
44 in Advanced LIGO data. *Physical Review D*, 104(10):102004, 2021.
- 45 [35] Soumya D. Mohanty and Ethan Fahnstock. Adaptive spline fitting with particle swarm
46 optimization. *Computational Statistics*, pages 1–37, 2020.
- 47 [36] Carl de Boor. On calculating with B-splines. *Journal of Approximation Theory*, 6(1):50 – 62,
48 1972.
- 49 [37] Svante Wold. Spline functions in data analysis. *Technometrics*, 16(1):1–11, 1974.
- 50 [38] Hermann G Burchard. Splines (with optimal knots) are better. *Applicable Analysis*, 3(4):309–319,
51 1974.
- 52 [39] David LB Jupp. Approximation to data by splines with free knots. *SIAM Journal on Numerical
53 Analysis*, 15(2):328–343, 1978.
- 54 [40] Zhen Luo and Grace Wahba. Hybrid adaptive splines. *Journal of the American Statistical
55 Association*, 82(398):461–471, 1987.
- 56
- 57
- 58
- 59
- 60

1
2 *Adaptive spline glitch removal*
3
45 *Association*, 92(437):107–116, 1997.

- 6 [41] Satoshi Miyata and Xiaotong Shen. Adaptive free-knot splines.
- Journal of Computational and*
-
- 7
- Graphical Statistics*
- , 12(1):197–213, 2003.
-
- 8 [42] Akemi Gálvez and Andrés Iglesias. Efficient particle swarm optimization approach for data fitting
-
- 9 with free knot b-splines.
- Computer-Aided Design*
- , 43(12):1683–1692, 2011.
-
- 10 [43] Soumya D. Mohanty. Particle swarm optimization and regression analysis I.
- Astronomical Review*
- ,
-
- 11 7(2):29–35, 2012.
-
- 12 [44] J. Kennedy and R. C. Eberhart. Particle swarm optimization. In
- Proceedings of the IEEE*
-
- 13
- International Conference on Neural Networks: Perth, WA, Australia*
- , volume 4, page 1942.
-
- 14 IEEE, 1995.
-
- 15 [45] Soumya D. Mohanty.
- Swarm Intelligence Methods for Statistical Regression*
- . Chapman and
-
- 16 Hall/CRC, 2018.
-
- 17 [46] Andries P Engelbrecht.
- Fundamentals of computational swarm intelligence*
- , volume 1. Wiley
-
- 18 Chichester, 2005.
-
- 19 [47] Daniel Bratton and James Kennedy. Defining a standard for particle swarm optimization. In
-
- 20
- Swarm Intelligence Symposium, 2007. SIS 2007. IEEE*
- , pages 120–127. IEEE, 2007.
-
- 21 [48] Hirotugu Akaike. Information theory and an extension of the maximum likelihood principle. In
-
- 22
- Selected Papers of Hirotugu Akaike*
- , pages 199–213. Springer, 1998.
-
- 23 [49] S Mukherjee. Median-based noise floor tracker (MNFT): robust estimation of noise floor drifts in
-
- 24 interferometric data.
- Classical and Quantum Gravity*
- , 20(17):S925, 2003.
-
- 25 [50] Michele Vallisneri, Jonah Kanner, Roy Williams, Alan Weinstein, and Branson Stephens. The
-
- 26 LIGO open science center. In
- Journal of Physics: Conference Series*
- , volume 610, page 012021.
-
- 27 IOP Publishing, 2015.
-
- 28 [51] Scott Coughlin, Michael Zevin, Sara Bahaadini, Neda Rohani, Sara Allen, Christopher Berry,
-
- 29 Kevin Crowston, Mabi Harandi, Corey Jackson, Vicky Kalogera, Aggelos Katsaggelos, Vahid
-
- 30 Noroozi, Carsten Osterlund, Oli Patane, Joshua Smith, Siddharth Soni, and Laura Trouille.
-
- 31 Gravity Spy Machine Learning Classifications of LIGO Glitches from Observing Runs O1, O2,
-
- 32 O3a, and O3b, Zenodo v1.0.0
- <https://doi.org/10.5281/zenodo.5649212>
- , November 2021.
-
- 33 [52] Brian McFee, Colin Raffel, Dawen Liang, Daniel P Ellis, Matt McVicar, Eric Battenberg, and
-
- 34 Oriol Nieto. librosa: Audio and music signal analysis in python. In
- Proceedings of the 14th*
-
- 35
- python in science conference*
- , volume 8, pages 18–25, 2015.
-
- 36 [53] Matlab Release2020b.
- The MathWorks, Inc., Natick, Massachusetts, United States.*
- ;
-
- 37
- <http://www.mathworks.com/>
- .
-
- 38 [54] Soumya D. Mohanty. Spline based search method for unmodeled transient gravitational wave
-
- 39 chirps.
- Physical Review D*
- , 96:102008, Nov 2017.
-
- 40 [55] S. D. Mohanty. Detection and estimation of unmodeled chirps. In
- 2018 26th European Signal*
-
- 41
- Processing Conference (EUSIPCO)*
- , pages 2643–2647, Sep. 2018.
-
- 42 [56] Soumya D. Mohanty. Glitch subtraction with adaptive spline – Part 1 [Data set], Zenodo v1
-
- 43
- <https://doi.org/10.5281/zenodo.7592442>
- , February 2023.
-
- 44
-
- 45
-
- 46